Magnetic anisotropy in permalloy: Hidden quantum mechanical features

Debora C. M. Rodrigues
Department of Physics and Astronomy, Uppsala University, Box 516, SE-751 20 Uppsala, Sweden and Faculdade de Física, Universidade Federal do Pará, CEP 66075-110, Belém-PA, Brazil

Angela B. Klautau
Faculdade de Física, Universidade Federal do Pará, CEP 66075-110, Belém-PA, Brazil

Alexander Edström, Jan Rusz, Lars Nordström, Manuel Pereiro, Björgvin Hjörvarsson, and Olle Eriksson
Department of Physics and Astronomy, Uppsala University, Box 516, SE-751 20 Uppsala, Sweden

(Received 20 February 2017; revised manuscript received 5 May 2018; published 4 June 2018)

By means of relativistic, first principles calculations, we investigate the microscopic origin of the vanishingly low magnetic anisotropy of Permalloy, here proposed to be intrinsically related to the local symmetries of the alloy. It is shown that the local magnetic anisotropy of individual atoms in Permalloy can be several orders of magnitude larger than that of the bulk sample and 5–10 times larger than that of elemental Fe or Ni. We furthermore show that locally there are several easy axis directions that are favored, depending on local composition. The results are discussed in the context of perturbation theory, applying the relation between magnetic anisotropy and orbital moment. Permalloy keeps its pronounced soft ferromagnetic nature due to the exchange energy to be larger than the magnetocrystalline anisotropy. Our results shine light on the magnetic anisotropy of permalloy and of magnetic materials in general, and in addition enhance the understanding of pump-probe measurements and ultrafast magnetization dynamics.

DOI: 10.1103/PhysRevB.97.224402

I. INTRODUCTION

Random alloys can be viewed as a distribution of clusters of different composition that have an underlying crystal structure in common. The configurational space is enormous for these systems and any macroscopic property is the result of averaging of a immense amount of local clusters with different configuration and composition [1]. Random alloys often have properties that stand out from the pure elements they are build up from, i.e., the mixing of elements may produce properties that are completely unexpected. One of the most prominent examples is Permalloy (Py), the common name for Fe_xNi_{1-x} alloys with $x \sim 0.2$ and fcc crystal structure. These alloys are characterized by strong ferromagnetism, high permeability, vanishingly low magnetic anisotropy energy (MAE), and low damping parameter [2]. These attributes elevate Py to a standard material in magnetism and advantageous soft magnet for technological applications.

One might ask what the mechanism of the vanishing MAE of Py really is. One attempt to explain it is the resultant MAE picture [3], which suggests that an appropriate mixture of two elements with distinct easy axis (as bcc Fe and fcc Ni with ⟨001⟩ and ⟨111⟩ direction, respectively) would result in a material without strong preferential easy magnetization axis. In this model each Fe and Ni atom maintains a finite, local anisotropy given by each element, producing a heterogeneous distribution of competing easy axis directions in which Fe always favors ⟨001⟩ and Ni always favors ⟨111⟩ easy axis direction. In this picture the vanishing anisotropy is realized by the exchange interaction dominating the magnetic anisotropy (which is generally true for 3*d* transition metals), combined with a competition of easy axis directions between Fe and Ni atoms.

This model, however, neglects the fact that elements when put into an alloy or compound interact and change the electronic structure and therefore, in principle, all observable properties. In line with this reasoning, experiments actually suggest that the Fe-Ni hybridization produces a unique electronic structure of Py and that this is the major cause of the low MAE [4]. Other experiments show the existence of orbital moments of the individual chemical species in Py [5]. Since it is known that the magnetic anisotropy is proportional to the anisotropy of orbital moment for transition metals [6,7], these results point to a potentially complex explanation for the vanishing MAE of Py.

As a random alloy, Py may be viewed as a huge ensemble of interconnected clusters of Fe-Ni atoms distributed on an fcc lattice, in which the macroscopic properties reflect the configurational average of different such clusters. Then different parts of the alloy may indeed have competing local anisotropies, that effectively average out, leading to a fairly isotropic state. Details of such a microscopic scenario has, to the best of our knowledge, not been considered so far as a possible mechanism for low MAE in Py. In the present work, we present first principles calculations to investigate this local MAE. However it is not easy to directly study the MAE, particularly not from first principles theory as it is hard to uniquely and accurately decompose the energy into local contributions and the numerical challenges are countless. Instead we will study another related quantity induced by the

spin-orbit coupling (SOC), namely, the local anisotropy of the orbital moment. It is well known to reveal information about the MAE [6]. With this information we investigate the role of these local competing anisotropies and their relevance for the soft magnetic behavior of Py.

II. METHOD

The study was designed as the following: First, we performed *ab initio* calculations of a fcc matrix (∼12 500 atoms) of a virtual crystal approximation (VCA) medium of Py (Py-VCA) and lattice parameter of 3.54 Å [5]. The fcc matrix was considered to have the same number of valence electrons as Py (9.6 e^-). After the self-consistent procedure, clusters composed by Fe and Ni, with different configurations, were embedded in the Py-VCA matrix. The cluster region was self-consistently updated while the potential parameters of the Py-VCA matrix were kept fixed.

The electronic structure and magnetism of VCA-Py and the clusters were evaluated using the first-principles real-space linear muffin-tin orbital method within the atomic sphere approximation (RS-LMTO-ASA) [8–11]. This method follows the steps of the LMTO-ASA formalism [12] but uses the recursion method [13] to solve the eigenvalue problem directly in real space. The calculations presented here are fully self-consistent, the exchange and correlation terms were treated within the local spin density approximation (LSDA) [14], and the SOC term was included at each variational step [15,16]. The RS-LMTO-ASA method is particularly designed to treat low symmetry systems as the embedded clusters presented here, without the need of periodic boundary conditions.

Since we use an electronic structure method that adopts the atomic sphere approximation, it is natural and expedient to make a projection of atomic contributions to the magnetic spin and orbital moment as well as the magnetic anisotropy. This was indeed done for every atom on each of the clusters we considered. We note that the atomic sphere approximation replaces the Wigner-Seitz cell with a sphere of equal volume [12]. As outlined [17] this allows us to define, even for an itinerant electron system, an effective spin Hamiltonian with atomic contributions to spin and orbital moments, interatomic exchange interactions, and a local contribution to the magnetic anisotropy. In the present work we evaluated the magnetic anisotropy from the anisotropy of the orbital moment, as detailed below, but we note that other methods exist in making atomic projected estimates of the magnetic anisotropy. For instance, in Ref. [18] the local anisotropy was determined from differences in the valence band energy projected on orbitals inside an atomic sphere.

Concerning the embedded clusters, we considered a central atom with its first and second neighboring shells allowing hence for 19 atomic positions in each cluster. The configuration space here is vast and any practical investigation cannot cover all possible configurations. We have, however, investigated as large a number of geometries that is practical (100 configurations, excluding symmetric geometries). Figures 1(a) and 1(b) show the average Fe and Ni occupation for each of the 19 sites in the clusters, for the case the smallest (8) and largest (100) number of configurations, respectively. The latter number of clusters is sufficient to produce average occupations of the

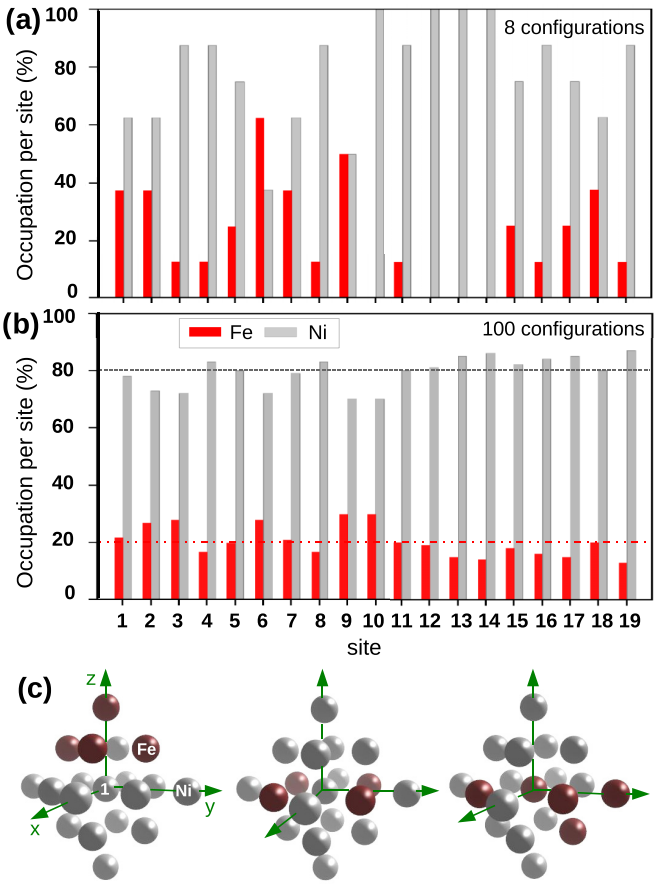

FIG. 1. Distributions of Fe (red) and Ni (gray) atoms at different cluster sites (the atom at the central site is numbered 1, atoms positioned on nearest neighbor positions are numbered 2–13, and atoms on second neighbor positions have numbers 14–19), considering (a) 8 or (b) 100 configurations. The dashed (dot-dashed) line represents the average Fe (Ni) concentration of Permalloy. Three examples of configurations that may be found in Permalloy are illustrated in (c). The gray spheres represent Ni atoms and red spheres Fe atoms.

different atomic sites that agree with what one expects for the average occupation of Py. We illustrate as an example a few typical geometries in Fig. 1(c), where the atoms are sorted from a central site (labeled 1), followed by its first (labeled 2–13) and second neighbors (labeled 14–19).

These clusters present distinct configurations due to the Fe content (composition) and distribution (arrangement at different sites). Note that, locally in a cluster, the number of Fe and Ni atoms can vary, although a configurational average over all clusters of the material would naturally result in a concentration of Fe and Ni that reflects the alloy concentration, i.e., 20% Fe and 80% Ni [marked as dashed lines in Fig. 1(b)].

By the binomial distribution, it is straightforward to calculate the probability of finding a specific concentration. We find that two Fe atoms ($x = 2$) distributed over the 19 cluster sites has a probability of 15%, when considering that the average concentration of Fe atoms in the alloy is 20%. In the same way we find that the probabilities of $x = 3$, 4, and 5 are 22%, 22%, and 16%, respectively. Hence we selected for our calculations clusters with these Fe concentrations and in this way our study embodies a sampling from 75% of all possible compositions.

We selected the following number of cluster geometries for each Fe concentration: For $x = 2$ we carried out a maximum of five different distributions of the Fe atoms, for $x = 3$ we considered 11 geometries, for $x = 4$ the number of clusters was 49, and for $x = 5$ we considered 35 different distributions of Fe atoms. This means that a maximum of 100 different clusters were considered in our electronic structure calculations. We note here that even though the binomial distribution gives similar concentrations for $x = 2$ and $x = 5$, we considered a larger number of geometries for $x = 5$ since the binomial coefficient is larger for this value of x. A similar reasoning was adopted for $x = 3$ and 4.

Regarding the calculations for the matrix of VCA-Py, the resulting spin moment (m_s) is 1.12 μ_B per atom, which is in acceptable agreement with the experimental value of approximately 1.0 μ_B per atom [4,5] and previous calculations [4,19,20]. Therefore, we conclude that the effective medium, considered to host the different clusters, reproduces the main features of Py.

For the different clusters in this investigation we have estimated the local anisotropy from a well defined quantity—the orbital moment anisotropy, which is the difference of the orbital moment projection L for two different global quantization axes $\Delta L = L_{\hat{\mathbf{n}}_1} - L_{\hat{\mathbf{n}}_2}$. Since ΔL is defined as a local quantity, it is numerically easy to evaluate from first principles theory in contrast to the tiny energy difference needed for the MAE. It is established that the energy difference between two states with the magnetization direction along two different global directions is $E_{\mathrm{MAE}} = -\frac{\xi}{4\mu_B}\Delta L$ [6,21], where ξ is the SOC constant. One of the key assumptions in deriving this relation is that spin diagonal matrix elements of the spin orbit coupling should dominate the contribution to the MAE [22]. Since Py is a strong ferromagnet (the majority spin band is essentially filled) only minority spin states contribute significantly to the density of states at the Fermi energy, and this criterion is expected to be fulfilled. In this situation, the easy axis is parallel to the direction of maximum orbital magnetic moment. To exemplify the numerical advantage of the approach adopted here, we note that values of 1 μRy for the MAE are related to orbital anisotropies of 10^{-4} μ_{B}, which are values well defined by the method's precision. Thus, it serves well as the relevant quantity to evaluate and to quantify the local anisotropies in alloys.

III. RESULTS AND DISCUSSIONS

Before we discuss the results of the MAE, we note that for all configurations investigated here, the calculated individual moments were close to $m_s^{Fe} = 2.30$ μ_{B} and $m_s^{Ni} = 0.61$ μ_{B} for spin moment and $L^{Fe} = 0.045$ μ_{B} and $L^{Ni} = 0.031$ μ_{B} for orbital moment. These values are in agreement with previous theoretical [19,20] and experimental [5] studies.

A. Site resolved easy axis and E_{MAE}

Next, we focus on the local magnetic anisotropy axis. For that, first we estimated the ΔL, between two magnetization directions for each atom, using orbital moments computed fully self-consistently.

The orbital moment anisotropy was computed as $\Delta L = L_{[001]} - L_{\hat{\mathbf{n}}_2}$, with $\hat{\mathbf{n}}_2 = [110]$ and $[111]$ directions. Comparing

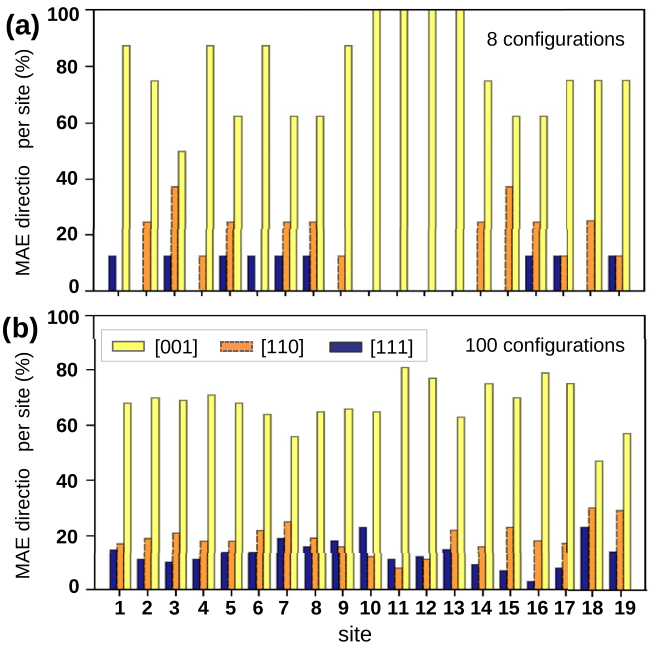

FIG. 2. Likelihood of different easy axis directions for each of the atomic sites from the clusters. Averages are formed from eight configurations (a) and 100 configurations (b). The easy axis direction are represented by the color bars.

the ΔL values one can obtain the direction that yields the maximum value of L, i.e., the easy axis of each atom in any of the clusters we considered. Hence we are able to find a distribution of probabilities of local easy axis orientations for the 19 atomic sites in the clusters we have considered here. This information is summarized in Fig. 2. In Fig. 2(a) we show results from eight different clusters (in this case we only considered values of x—the number of Fe atoms—of 3 and 4) and in Fig. 2(b) 100 different configurations. We note that the easy axis orientations along [110] and [111] directions have a relative increase if more configurations are considered [compare Figs. 2(a) and 2(b)]. We also note that the probability of finding [110] and [111] easy axis directions is more or less equally high, which is what one should expect for a material with a vanishing global magnetic anisotropy. However, Fig. 2 shows that the probability of finding the [001] easy axis orientation is somewhat too high, if one has in mind that the global magnetic anisotropy should be vanishingly small. The tendency of density functional theory in the local density approximation or the generalized gradient approximation to favor the [001] direction of fcc Ni is well known [23], and it is possible that the results shown in Fig. 2 reflect a similar situation. The general trends and the analysis provided in this paper would not be changed qualitatively if the functional used resulted in a perfect distribution of probabilities of local easy axis orientations.

In addition to these values of ΔL we also estimated the site resolved E_{MAE}. For that, we used the calculated SOC constants for $\xi_{\mathrm{Fe}} = 4.0$ mRy and $\xi_{\mathrm{Ni}} = 6.7$ mRy. The values of E_{MAE} and the direction of the easy axis for each atom are shown in Fig. 3 (for sake of simplicity only eight configurations are shown). Note from the figure that we find local easy axis

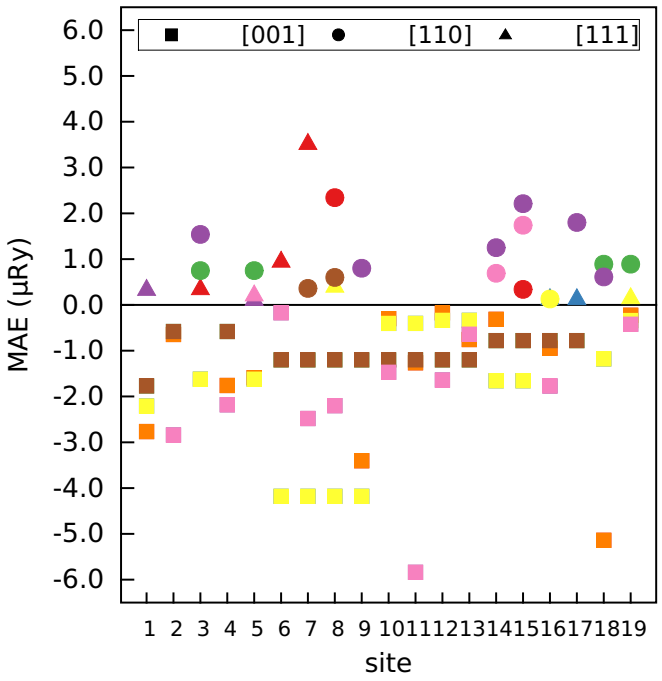

FIG. 3. MAE per site with the easy axis direction represented by squares (for [100]), circles (for [110]) and triangles (for [111] direction). Note that negative values of the MAE symbolize an [001] easy axis, while positive values symbolize that the [111] or [110] direction was an easy axis. The eight different configurations considered here are represented by different colors. Note that some data points are superposed, since the same MAE value is found for an atom placed in a given site of different configurations.

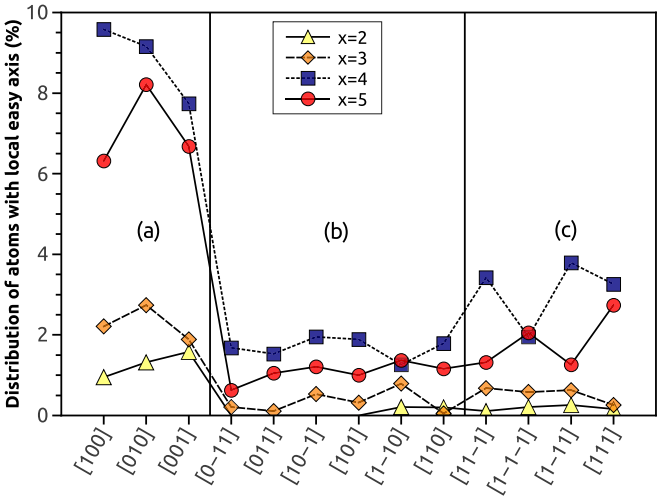

FIG. 4. Distribution of atomic sites with easy axis pointing in any of the 13 possible cubic crystalline directions (see text). The calculations made use of the force theorem and considered 100 configurations. The symbols stand for different Fe compositions of the clusters.

directions that in general are different for each atom in the cluster. The figure also shows that different configurations in general have very different local anisotropies. For instance, the eight clusters considered in this figure all have rather different behaviors when it comes to the MAE. For some of them, e.g., site 3 in one cluster can have the [100] easy axis direction, but other configurations could favor the [110] or the [111] easy axis direction for this site. Although not shown in Fig. 3, we find no clear trend for the Fe and Ni atoms, for different clusters and different sites, both atom types can have any of the three considered local easy axis orientations. As is clear from the figure we find values that are typically 5–10 times larger compared to the values of bcc Fe (∼0.1 μRy) or fcc Ni (∼0.2 μRy) [24]. Further, these local MAE values are, remarkably, orders of magnitude larger compared to the almost vanishing value of the MAE of bulk Py.

A key point of Fig. 3 is that the symmetry of each cluster is not cubic. Hence, spin-orbit effects enter as a local uniaxial anisotropy and it depends on second-order anisotropy terms instead of fourth-order contributions that are expected from cubic environments. This is the primary reason why the local MAE values of Py are bigger than those of bcc Fe and fcc Ni.

It is interesting to compare the results of Figs. 2 and 3 to recent supercell calculations for the MAE of FeCo based alloys [25,26]. There it is also found that the local anisotropy of various atomic configurations varies strongly, and even changes sign, while the alloy MAE is described by the average over many configurations. Those systems are, however, very different in that they have a large MAE, meaning that one direction of magnetization should be over-represented among different cluster configurations. Py differs in that the MAE is vanishingly small, meaning that there must be a balance from different local anisotropy contributions.

B. Easy axis distribution

Considering that local electronic properties of atoms in Py are distinct, the atomic easy axis may point in a particular direction among any of the 26 orientations of the cubic lattice (that is to say ⟨001⟩, ⟨110⟩, and ⟨111⟩). For instance, the ⟨001⟩ direction actually represents six equivalent directions in a homogeneous environment, however, in a disordered alloy, there is no such constraint. Therefore, we considered a complementary statistical analysis considering the 26 axis directions as independent. For that, we computed L for all 26 directions, from which we extracted values of ΔL, having the [001] axis as reference (note that we distinguish specific directions by writing them within square bracket). Here we applied the force-theorem method [27,28] in order to compute the orbital moments, with the advantage of good precision for MAE calculations [29,30] combined with computational efficiency. The obtained magnetic anisotropy energies are compatible with the ones computed from fully self-consistent calculations (shown in Fig. 3).

Figure 4 shows the calculated distribution of atoms with a given easy axis. These results were obtained from one hundred clusters with four different cluster compositions ($x = 2$, 3, 4, and 5), which means that the data in Fig. 4 represent 1900 atoms in total. It should be noted that of all these calculations we found no significant difference in orbital moment (or anisotropy energy) of a particular magnetic configuration and its time-reversed state, which is consistent with Kramers theorem. For this reason we plot in Fig. 4 the distribution of easy axis orientations of 13 directions, grouping together information

TABLE I. Distribution (in percent) of atomic sites with easy axis pointing in the ⟨001⟩, ⟨110⟩, and ⟨111⟩ direction. The data is presented for different values of Fe concentration, as well as the total sum of all Fe concentrations. The calculations made use of the force theorem and considered 100 configurations.

	$x = 2$	$x = 3$	$x = 4$	$x = 5$	total sum
⟨001⟩	3.85	7.05	28.16	21.84	60.9
⟨110⟩	0.41	1.80	8.42	5.79	16.42
⟨111⟩	0.74	2.15	12.42	7.37	22.68

from time-reversed states. Thus, each data point shown in Fig. 4 is the distribution of atoms (in percent) with an easy axis along a specific direction. The information in the figure also specifies which cluster composition the different calculations correspond to. Note that for a calculation employing a very large number of clusters one would expect the distribution of atoms with easy axis along [001] would be the same as that along [010] or [100]. This is not entirely reflected in the data shown in Fig. 4(a), due to the limited number of clusters (one hundred) used here. However, the degeneracy in the distribution for the different directions shown in Fig. 4(a) is rather close to expectations. A similar conclusion can be reached for the distribution of the other easy axis directions, shown in Figs. 4(b) and 4(c). Figure 4 also shows that clusters with higher local concentration of Fe ($x = 4$ and 5) are prone to have the easy axis point in the ⟨001⟩ or ⟨111⟩ directions, whereas the ⟨110⟩ directions have lower probability for all concentrations.

The data in Fig. 4 is summarized in Table I, where we have integrated the distributions along the ⟨001⟩, ⟨110⟩, and ⟨111⟩ directions. In the case of an isotropic scenario of the 13 possible directions, one would expect the following distribution of atoms with easy axis along the three-, six-, and fourfold axis: ⟨001⟩ with 23%, ⟨110⟩ with 46%, and ⟨111⟩ with 31%, respectively. Our calculations show a contribution of ⟨001⟩ directions that constitute 61% of the data, see Table I. This is related mainly to contributions from Ni atoms (data not shown).

The other calculated contributions are 16% from ⟨110⟩ directions and 23% of ⟨111⟩ directions (Table I). The calculations shown in Table I and Fig. 4 hence deviate from the expected behavior of a completely isotropic material, and as mentioned above this likely reflects the shortcoming of LDA or GGA functionals for fcc Ni and as this study demonstrated for Ni rich alloys.

IV. CONCLUSIONS

We consider here the magnetic anisotropy of a macroscopic sample as a configurational average of local anisotropies, for a diverse distribution of clusters like the ones shown in Fig. 1(c). Each cluster may have several atoms with large local anisotropies directed in any of the common crystallographic axes (⟨001⟩, ⟨110⟩, and ⟨111⟩), but since the interatomic exchange interaction of Py (not shown here) is much stronger and ferromagnetic, the resulting magnetic configuration is a collinear ferromagnet, where, after a proper configurational average is made, the resulting MAE is expected to be vanishingly small.

In this study, we only investigated clusters with approximately the same concentration of Fe and Ni as one has in Py ($Fe_{0.2}Ni_{0.8}$). In a real sample such constraint does not exist, and configurations involving, e.g., 1 Ni and 18 Fe atoms and vice versa also appear, albeit with low probability. Once a proper configurational average of a huge set of clusters is considered, the proper macroscopic MAE can be obtained, and we suggest this leads to a vanishingly small MAE for Py. The scenario proposed here is principally different than simply making a linear interpolation of anisotropy constants of bcc Fe and fcc Ni and adopting an interpolated value for all atoms of the alloy. This is particularly clear from the calculations that show that the local anisotropy is orders of magnitude larger than the observed anisotropy in Py. This naturally comes out from a consideration of the distribution of atoms in a typical cluster, where cubic symmetry is broken and hence the importance of spin-orbit effects enters at a much higher level. It is also clear from the theory that the Fe and Ni atoms can have local easy axis directions along the ⟨100⟩, ⟨110⟩, and ⟨111⟩ axis, depending on the local distribution of atoms. This is naturally a significantly more complex behavior, compared to a simple average of Fe and Ni atoms with fixed easy axis orientations.

We argue here that the vanishing anisotropy in bulk Py arises from the cancellation of these local anisotropies. It is likely that the scenario put forward here also applies to other magnetic parameters, like the damping parameter or potentially the asymmetric exchange (like a local Dzyaloshinskii-Moriya interaction). We also note that experiments showed that amorphous materials present orbital induced magnetic anisotropy [31,32] explained by the random anisotropy model. Note that in amorphous materials the lack of symmetry (chemical and crystalline) allows the emergence of orbital anisotropy. As a final comment, we note that the local anisotropy effects discussed here might affect the magnetization dynamics in thin films of Py [33]. For that, adopting a scenario of locally unique information, as proposed here, would be relevant for the interpretation of pump-probe measurements and crucial to simulations involving an effective spin Hamiltonian.

ACKNOWLEDGMENTS

D.C.M.R. thanks D. Thonig for insightful discussions. The authors acknowledge support from the Swedish Research Council (VR), the KAW foundation (Grant Nos. 2012.0031 and 2013.0020), STANDUPP, and eSSENCE. A.B.K. acknowledges support from CNPq (Brazil). D.C.M.R. acknowledges support from CAPES (Brazil) for financial support and "CENAPAD/UNICAMP" for providing computational facilities.

[1] I. A. Abrikosov, O. Eriksson, P. Söderlind, H. L. Skriver, and B. Johansson, Phys. Rev. B **51**, 1058 (1995).

[2] J. M. Coey, *Magnetism and Magnetic Materials* (Cambridge University Press, Cambridge, 2001).

[3] L. W. McKeehan, Phys. Rev. **52**, 18 (1937).
[4] L. F. Yin, D. H. Wei, N. Lei, L. H. Zhou, C. S. Tian, G. S. Dong, X. F. Jin, L. P. Guo, Q. J. Jia, and R. Q. Wu, Phys. Rev. Lett. **97**, 067203 (2006).
[5] B. Glaubitz, S. Buschhorn, F. Brüssing, R. Abrudan, and H. Zabel, J. Phys.: Condens. Matter **23**, 254210 (2010).
[6] P. Bruno, Phys. Rev. B **39**, 865 (1989); P. Bruno and J. P. Renard, Appl. Phys. A **49**, 499 (1989).
[7] R. Skomski, A. Kashyap, and A. Enders, J. Appl. Phys. **109**, 07E143 (2011).
[8] P. R. Peduto, S. Frota-Pessôa, and M. S. Methfessel, Phys. Rev. B **44**, 13283 (1991).
[9] S. Frota-Pessôa, Phys. Rev. B **46**, 14570 (1992).
[10] A. Bergman, L. Nordström, A. B. Klautau, S. Frota-Pessôa, and O. Eriksson, Surf. Sci. **600**, 4838 (2006).
[11] A. B. Klautau and S. Frota-Pessôa, Surf. Sci. **579**, 27 (2005).
[12] O. K. Andersen, Phys. Rev. B **12**, 3060 (1975).
[13] R. Haydock, in *Solid State Physics: Advances in Research and Applications*, edited by H. Ehrenreich, F. Seitz, and D. Turnbull (Academic Press, London, 1980), Vol. 35, p. 215.
[14] U. von Barth and L. A. Hedin, J. Phys. C: Solid State Phys. **5**, 1629 (1972).
[15] O. Eriksson, B. Johansson, R. C. Albers, A. M. Boring, and M. S. S. Brooks, Phys. Rev. B **42**, 2707 (1990).
[16] S. Frota-Pessôa, Phys. Rev. B **69**, 104401 (2004).
[17] O. Eriksson, A. Bergman, L. Bergqvist, and J. Hellsvik, *Atomistic Spin Dynamics: Foundations and Applications* (Oxford University Press, Oxford, 2017).
[18] G. H. O. Daalderop, P. J. Kelly, and M. F. H. Schuurmans, Phys. Rev. B **41**, 11919 (1990).
[19] P. Yu, X. F. Jin, J. Kudrnovský, D. S. Wang, and P. Bruno, Phys. Rev. B **77**, 054431 (2008).
[20] J. Minár, S. Mankovsky, O. Šipr, D. Benea, and H. Ebert, J. Phys.: Condens. Matter **26**, 274206 (2014).
[21] P. James, O. Eriksson, O. Hjortstam, and B. Johansson, and L. Nordström. Appl. Phys. Lett. **76**, 915 (2000).
[22] C. Andersson, B. Sanyal, O. Eriksson, L. Nordström, O. Karis, D. Arvanitis, T. Konishi, E. Holub-Krappe, and J. H. Dunn, Phys. Rev. Lett. **99**, 177207 (2007).
[23] J. Trygg, B. Johansson, and O. Eriksson, and J. M. Wills, Phys. Rev. Lett. **75**, 2871 (1995).
[24] S. V. Halilov, A. Y. Perlov, P. M. Oppeneer, A. N. Yaresko, and V. N. Antonov, Phys. Rev. B **57**, 9557 (1998).
[25] M. Dëne, S. K. Kim, M. P Surh, D. Åberg, and L. X. Benedict, J. Phys.: Condens. Matter **27**, 266002 (2015).
[26] S. Steiner, S. Khmelevskyi, M. Marsmann, and G. Kresse, Phys. Rev. B **93**, 224425 (2016).
[27] O. K. Andersen, H. L. Skriver, H. Nohl, and B. Johansson, Pure Appl. Chem. **52**, 93 (1980).
[28] V. Heine, in *Solid State Physics: Advances in Research and Applications*, edited by H. Ehrenreich, F. Seitz, and D. Turnbull (Academic Press, London, 1980), Vol. 35, p. 119.
[29] A. B. Klautau and O. Eriksson, Phys. Rev. B **72**, 014459 (2005).
[30] S. Abdelouahed and M. Alouani, Phys. Rev. B **79**, 054406 (2009).
[31] T. Hase, H. Raanaei, H. Lidbaum, C. Sánchez-Hanke, S. Wilkins, K. Leifer, and B. Hjörvarsson, Phys. Rev. B **80**, 134402 (2009).
[32] F. Magnus, R. Moubah, A. H. Roos, A. Kruk, V. Kapaklis, T. Hase, and B. Hjörvarsson, and G. Andersson, Appl. Phys. Lett. **102**, 162402 (2013).
[33] D. Mauri, D. Scholl, H. C. Siegmann, and E. Kay, Appl. Phys. A **49**, 439 (1989).